*IUBAT Review—A Multidisciplinary Academic Journal, 8(2): 82-104*
https://doi.org/10.3329/iubatr.v8i2.86881

# Electrochemical and Magnetic Behavior of a Thermally Stable Copper(II) Complex Bridged by Aspartate and Bipyridine Ligands

Saiful Islam[1]*, Md. Hafizul Islam[2] Mohammad Moniruzzaman[3], Dr. Md. Jahidul Islam[4]

[1]*Department of Chemistry, International University of Business Agriculture and Technology (IUBAT), Dhaka 1230, Bangladesh.*

[2]*Department of Chemistry, International University of Business Agriculture and Technology (IUBAT), Dhaka 1230, Bangladesh.*

[3]*Department of Psychiatry and Behavioral Health, Stony Brook University, Stony Brook, NY 11794-8101, USA.*

[4]*Department of Chemistry, International University of Business Agriculture and Technology (IUBAT), Dhaka 1230, Bangladesh.*

***Keywords:***

*Mixed-ligand copper(II) complex; Aspartic acid coordination; 4,4′-Bipyridine (bpy); Redox and magnetic properties; Electrochemical and thermal stability*

***Abstract***

*A novel mixed-ligand copper(II) complex, [Cu(Asp)(bpy)]·nH₂O, incorporating aspartic acid (Asp) and 4,4′-bipyridine (bpy), was synthesized and extensively characterized to elucidate its redox, magnetic, thermal, and spectroscopic properties. Fourier-transform infrared spectra confirmed coordination through the carboxylate oxygen of Asp and the nitrogen atoms of bpy, forming a mixed N,O-donor environment around the Cu(II) center. UV–Visible spectroscopy revealed d–d and metal-to-ligand charge transfer transitions, while fluorescence spectra displayed emission quenching due to the paramagnetic Cu(II) ion, confirming effective metal–ligand interaction. The complex exhibited an effective magnetic moment ($\mu_{eff}$) of 2.46 Bohr magnetons, consistent with a single unpaired electron in a distorted octahedral geometry. Thermogravimetric analysis indicated a multi-step decomposition pattern with stability up to 350 °C, suggesting strong metal–ligand coordination and potential thermal robustness. Electrochemical investigations using cyclic voltammetry demonstrated a quasi-reversible Cu(II)/Cu(I) redox couple, with diffusion-controlled kinetics and ligand-induced stabilization of the Cu(I) oxidation state. Molar conductivity measurements indicated the formation of a neutral complex, further confirming complete coordination. Collectively, these findings establish the structural integrity and multifunctional nature of the Cu–Asp–bpy complex. Owing to its redox reversibility, paramagnetic character, and high thermal stability, the complex shows promise for applications in electrocatalysis, redox-active materials, and bioinspired electron-transfer systems. This study provides valuable insight into how synergistic N,O-ligand coordination can modulate copper redox chemistry and enhance functional stability for*

*Corresponding author's E-mail address: dislam.chem@iubat.edu
Article received: September 2025 Revised and accepted: December 2025 Published: December 2025

*potential catalytic and electronic applications. These findings collectively demonstrate that the Cu–Asp–bpy complex possesses a stable Cu(II)/Cu(I) redox couple and high thermal durability, making it a promising candidate for electrocatalytic and bioinspired electron-transfer applications.*

## Graphical abstract

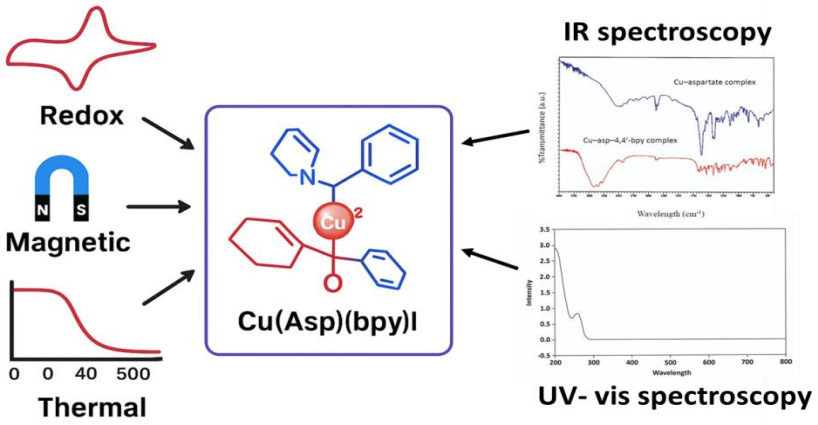


## 1. Introduction

Transition metal complexes continue to receive substantial attention in modern chemistry due to their diverse structural features, intriguing electronic properties, and broad range of applications in catalysis, materials science, medicine, and bioinorganic systems (Kainat *et al.*, 2024; Sahu & Sahu, 2024; Saiful *et al.*, 2020). Among transition metals, copper is particularly noteworthy due to its abundance, rich coordination chemistry, and the ability to adopt multiple oxidation states—primarily +1 and +2, and rarely 0 and +3. These properties make copper complexes ideal candidates for redox-active systems, electron-transfer mediators, and structural models for metalloproteins (Cheng, Wang, Wang, & Deng, 2018; Elwell *et al.*, 2017; Saiful *et al.*, 2022). Copper(II) complexes exhibit a wide variety of geometries depending on ligand field strength, coordination number, and the nature of donor atoms (Hoffmann *et al.*, 2016; Saiful *et al.*, 2022). In octahedral and square planar environments, the copper(II) ion ($Cu^{2+}$) adopts a [Ar] $3d^9$ electronic configuration (Aramburu, Garcia-Fernandez, Mathiesen, Garcia-Lastra, & Moreno, 2018; Chakrabarty, Mim, Tonu, Ara, & Dhar, 2024). This configuration leads to paramagnetic behavior, typically with one unpaired electron due to the splitting of d-orbitals in the ligand field (Ishii, Ogasawara, & Sakane, 2024; S. Islam *et al.*, 2025). In octahedral complexes, the Jahn-Teller effect often distorts the geometry, lowering symmetry and stabilizing the system, while square planar structures (common for $Cu^{2+}$) also retain one unpaired electron

(M. J. Islam & S. Islam, 2025; Shi *et al.*, 2024). The paramagnetism of $Cu^{2+}$ complexes can be quantified using magnetic susceptibility measurements (such as the Gouy method or Evans method), while their redox activity ($Cu^{2+} \rightleftharpoons Cu^{+}$) is studied via electrochemical techniques like cyclic voltammetry (K. S. Abou-Melha, 2024; K. S. A. Abou-Melha, 2025; M. J. Islam, Islam, & Islam, 2025a). These properties make $Cu^{2+}$ complexes important in catalysis, bioinorganic chemistry, and materials science (Shakdofa, Al-Hakimi, Elsaied, Alasbahi, & Alkwlini, 2017).

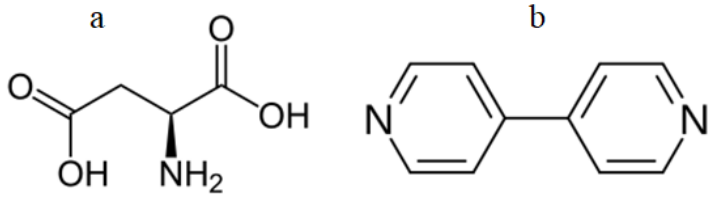


**Figure 1:** Schematic representation of the coordination environment of Cu(II) with aspartic acid and 4,4′-bipyridine ligands.

Amino acids are widely used as ligands in metal complexation due to their biocompatibility, versatile coordination modes, and relevance in biological and environmental systems (Maldonado & Amo-Ochoa, 2021; Marinova & Tamahkyarova, 2024; Rahman *et al.*, 2025). Among them, aspartic acid (Asp, $HOOC–CH(NH_2)–CH_2–COOH$) acts as a polydentate ligand, capable of coordinating through its amino ($–NH_2$) group and one or both carboxylate ($–COO^-$) groups (monodentate or bidentate binding) (Evans, Guevremont, & Rabenstein, 2024). This multifunctionality allows Asp to participate in chelation or bridging interactions, making it crucial in metalloprotein active sites, where metal ions are stabilized by hydrogen bonding, electrostatic interactions, and coordination bonds within the protein scaffold (Kozlowski, Potocki, Remelli, Rowinska-Zyrek, & Valensin, 2013; F. Yu *et al.*, 2014). Aspartic acid's flexible binding modes and high affinity for transition metals (e.g., $Cu^{2+}$, $Zn^{2+}$, $Fe^{3+}$) render it valuable for designing bioinspired complexes with potential applications in catalysis, medicinal chemistry, and environmental remediation (Chakrabarty *et al.*, 2023; Marinova & Tamahkyarova, 2024; Swain, Kar, & Misra, 2025). The rigid, planar 4,4′-bipyridine (bpy) ligand serves as a versatile building block in coordination chemistry due to its linear bidentate structure that readily bridges metal centers to construct extended frameworks, supramolecular assemblies, and heteroleptic complexes (Cook, Zheng, & Stang, 2013; Sharmin, Islam, Hanif, Islam, & Islam, 2025) Figure 1**.** This nitrogen-donor ligand plays a crucial role in tuning the electronic properties of metal centers by stabilizing oxidation states, enhancing metal-to-ligand charge transfer transitions, and improving complex stability through chelation effects (Diana & Panunzi, 2020; M. J. Islam, Islam, & Islam, 2025b). When combined with aspartic acid - an oxygen-donor ligand offering pH-dependent coordination modes and hydrogen bonding capability - in

copper(II) complexes, the system enables investigation of synergistic ligand interactions (Lukács, Szyrwiel, & Pap, 2019). This unique combination allows exploration of cooperative effects on redox behavior, magnetic exchange coupling between metal centers, and electronic communication in polymeric architectures, while the Jahn-Teller active Cu(II) center provides additional geometric and electronic variability to probe structure-property relationships (H. Islam, Islam, & Harun-Ur-Rashid; Schwiedrzik, 2023). Previous studies have extensively characterized the redox properties of copper complexes through cyclic voltammetry, establishing clear correlations between ligand architecture and electrochemical parameters such as redox potential ($E_{1/2}$) and electron transfer kinetics (Aoki, Chen, Liu, & Jia, 2020). Complementary magnetic susceptibility measurements have proven valuable for elucidating the oxidation state of copper centers and distinguishing between mononuclear (S = 1/2) and antiferromagnetically coupled binuclear (S = 0) species, as well as identifying geometry-dependent effects (e.g., Jahn-Teller distortions in octahedral vs. square planar Cu(II) complexes) (Roy, Mitra, & Patra, 2011). However, despite these advances, systematic investigations of hybrid systems combining biologically relevant amino acid ligands with rigid N,N′-bidentate spacers like 4,4′-bipyridine remain underexplored. Such studies are becoming increasingly important for developing fundamental structure-property relationships in these multifunctional systems, particularly for applications in bioinspired catalysis (e.g., mimicking copper oxidase active sites), molecular electronics (charge transport materials), and chemosensing platforms (selective metal ion detection). (Ede, Yu, Sung, & Kisailus, 2024; Xing *et al.*, 2025). In contrast to previously reported Cu–amino acid–bipyridine systems, the present study introduces a distinct ligand environment that combines the hard O-donor sites of aspartic acid with the rigid N-donor framework of 4,4′-bipyridine in a single coordination platform. This mixed N,O-donor arrangement has not been systematically explored in terms of its integrated structural, electrochemical, and magnetic consequences. Moreover, unlike earlier studies that focused primarily on spectral or structural characterization, our work provides a comprehensive correlation between ligand coordination mode, ligand-field effects, quasi-reversible Cu(II)/Cu(I) redox behavior, and magnetic parameters. This establishes the novelty of the Cu–Asp–bpy complex and highlights its significance as a unique hybrid system within the broader family of copper amino-acid–bipyridine complexes.

In this context, we report the synthesis and physicochemical characterization of a novel copper(II) complex, Copper(II) Aspartate–4,4′-Bipyridine Complex(Cu–Asp–bpy), coordinated with aspartic acid and 4,4′-bipyridine ligands. The structural features of the complex were probed using spectroscopic and analytical techniques, while its redox behavior was investigated through cyclic voltammetry at varying scan rates to evaluate electron transfer reversibility and kinetic behavior. Magnetic susceptibility was measured using a substituted Gouy balance, enabling us to calculate the effective magnetic moment and deduce the coordination geometry and purity of the sample. Through this combined

electrochemical and magnetic study, we aim to provide comprehensive insight into the structure–property relationships of this mixed-ligand copper complex, contributing to the broader understanding of copper coordination chemistry with biological and functional ligands.

Therefore, the primary objectives of this study are: (i) to synthesize a new mixed-ligand Cu(II) complex incorporating aspartic acid and 4,4′-bipyridine, (ii) to elucidate its structural, spectroscopic, electrochemical, magnetic, and thermal characteristics, and (iii) to establish correlations between these physicochemical properties and its potential functional applications.

## 2. Materials and Methods

### 2.1. Chemicals and Reagents

All chemicals and solvents were of analytical reagent (AR) grade and used without further purification unless otherwise stated. Copper(II) chloride dihydrate ($CuCl_2 \cdot 2H_2O$, ≥99%, Merck), L-aspartic acid (≥99%, Sigma–Aldrich), and 4,4′-bipyridine (≥98%, Sigma–Aldrich) were purchased from commercial suppliers. Deionized water was used for all solution preparations.

### 2.2. Synthesis of the Cu(II)–Aspartate–4,4′-Bipyridine Complex

The Cu–Asp–bpy complex was synthesized by a solution-based method under ambient conditions. In a 100 mL round-bottom flask, copper(II) chloride dihydrate (0.34 g, 2.0 mmol) and L-aspartic acid (0.27 g, 2.0 mmol) were dissolved in 40 mL of deionized water with continuous magnetic stirring at 70–80 °C for 30 min, producing a clear bluish-green solution of copper(II) aspartate. The pH of the reaction mixture was maintained near 6.0 using dilute NaOH to ensure complete dissolution of aspartic acid and effective complexation with Cu(II). After cooling the solution to room temperature, 4,4′-bipyridine (0.63 g, 4.0 mmol; 4.0 mL of 0.1 M ethanolic solution) was added dropwise with stirring, which caused a gradual color change from green to deep blue, indicating the formation of the mixed-ligand complex. The reaction mixture was stirred for an additional 2 h at room temperature, filtered to remove any insoluble residue, and left undisturbed in a refrigerator at 5–7 °C for 48 h. The resulting light-blue crystalline product was collected by vacuum filtration, washed several times with small portions of cold deionized water followed by ethanol to remove unreacted ligands, and dried at room temperature between filter papers. The dried product was stored in a desiccator over silica gel until further use. The yield was 0.78 g (56% based on copper). The complex was moderately soluble in water and methanol, sparingly soluble in hot acetone, and insoluble in ethanol, consistent with its neutral molecular character and strong metal–ligand coordination.

### 2.3. Instrumentation and Analytical Methods

All physicochemical characterizations were performed using standard analytical instruments to confirm the structural and electronic features of the synthesized complex. Fourier-transform infrared (FT-IR) spectra were recorded in the range of

4000–400 $cm^{-1}$ on a Bruker Alpha II spectrometer using KBr pellets. UV–Visible absorption spectra were obtained with a Shimadzu UV-2600 spectrophotometer in aqueous medium ($1 \times 10^{-3}$ M) at ambient temperature, while fluorescence spectra were measured on a Shimadzu RF-6000 spectrofluorometer with an excitation wavelength of 340 nm. Magnetic susceptibility measurements were carried out at room temperature using a Sherwood Scientific Magnetic Susceptibility Balance (UK), calibrated with $Hg[Co(SCN)_4]$, to determine the effective magnetic moment ($\mu_{eff}$). Molar conductivity was determined at 298 K using a Jenway 4510 conductivity meter to evaluate the electrolyte nature of the complex. Thermogravimetric analysis (TGA) was performed on a PerkinElmer STA 6000 system under a nitrogen atmosphere at a heating rate of 10 °C $min^{-1}$ to assess the thermal stability and decomposition pattern. Electrochemical studies were conducted on a CHI 660E electrochemical workstation (CH Instruments, USA) using a conventional three-electrode setup consisting of a glassy carbon working electrode, platinum counter electrode, and Ag/AgCl reference electrode, with 0.1 M KCl serving as the supporting electrolyte.

## 3. Results and Discussion

### 3.1. Infrared Spectroscopic Characterization

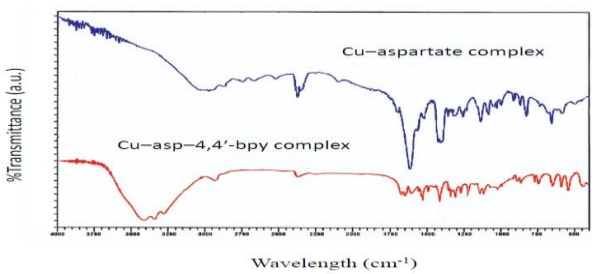


**Figure 2:** Comparative FT-IR spectra of Cu–Asp and Cu–Asp–bpy complex showing major shifts in carboxylate and pyridyl stretching bands

FT-IR spectroscopy was used to probe ligand coordination in the aspartate and mixed-ligand Cu(II) assemblies. The IR overlay (Figure 2) shows several systematic changes on formation of the Cu–Asp–bpy complex relative to the Cu–aspartate precursor. The broad band near 3400 $cm^{-1}$ in both materials is assigned to ν(OH) of coordinated/ hydrogen-bonded water and N–H stretching; its pronounced breadth in the complexes is consistent with the presence of coordinated water molecules and intermolecular hydrogen bonding (M. H. Islam *et al.*, 2024). The sharp ν(C=O) band expected for a free carboxylic acid (≈1700–1725 $cm^{-1}$) is absent in both complex spectra, indicating deprotonation of the carboxyl group(s) and formation of carboxylate species. Strong absorptions in the 1600–1400 $cm^{-1}$ region are therefore assigned to the asymmetric and symmetric stretches of coordinated carboxylate, $\nu_{as}(COO^-)$ and $\nu_{s}(COO^-)$, respectively. From the measured peak positions (Table 1) $\Delta\nu = \nu_{as}(COO^-) - \nu_{s}(COO^-)$ is ≈ 222 $cm^{-1}$

(approx., see Table 1), a magnitude more consistent with an asymmetric monodentate or bridging coordination mode of the carboxylate to Cu(II) rather than a symmetric bidentate chelate. Incorporation of 4,4′-bipyridine is evidenced by additional bands and increased intensity in the 1600–1500 $cm^{-1}$ region together with multiple ring-breathing features in the 1000–700 $cm^{-1}$ window, attributable to pyridyl ring stretching and C=N modes; these bands are either absent or much weaker in the Cu–aspartate spectrum. In the low-frequency region (≈500–350 $cm^{-1}$) new bands consistent with ν(M–O) and ν(M–N) are observed for the bpy-containing complex, confirming a mixed N,O coordination environment (Cu–O from aspartate and Cu–N from bpy) (M. J. Islam & M. H. Islam, 2025a, 2025b; Sharmin, Islam, & Islam, 2025). Collectively, the IR data support a structural picture in which aspartate coordinates to Cu(II) primarily through deprotonated carboxylate oxygen(s) while 4,4′-bipyridine binds through its pyridyl nitrogens, with coordinated water molecules completing the coordination sphere. These conclusions are consistent with a change in carboxylate binding mode upon bpy coordination and should be corroborated by single-crystal X-ray diffraction and EPR spectroscopy for definitive geometric and electronic characterization.

**Table 1:** Characteristic FT-IR Absorption Bands and Vibrational Assignments for the Cu–Asp and Cu–Asp–bpy complex

| Band | Assignment | Observed ($cm^{-1}$) peak position | Notes |
|---|---|---|---|
| ~3400 | ν(OH, $H_2O$) / ν(N–H) (broad) | 3420 (both samples) | Broad; indicates coordinated water / H-bonded N–H |
| (free COOH) ~1700 | ν(C=O) free carboxylic acid | absent / very weak | Loss → deprotonation on coordination |
| $\nu_{as}(COO^-)$ | asymmetric carboxylate stretch | 1608 (Cu–asp–bpy) / 1598 (Cu–asp). | Primary diagnostic band for $COO^-$ |
| $\nu_s(COO^-)$ | symmetric carboxylate stretch | 1386 (both). | Use to compute Δν |
| $\Delta\nu = \nu_{as} - \nu_s$ | Carboxylate coordination indicator | ≈ 222 $cm^{-1}$ | Value suggests monodentate / asymmetric bridging mode |
| 1600–1500 | Pyridine C=N / aromatic ring modes (bpy) | 1585–1505 (Cu–asp–bpy) | Confirms bpy incorporation and N→Cu coordination |
| 1000–700 | Ring-breathing / out-of- | 820, 760, 720 | Characteristic aromatic |

| | | | |
|---|---|---|---|
| | plane modes (bpy) | (Cu–asp–bpy) | fingerprint of bpy |
| 500–350 | ν(M–O), ν(M–N) (metal–ligand) | 480, 420 | Confirms mixed Cu–O / Cu–N coordination in bpy complex |

### 3.2. UV–Visible Spectral Features and Electronic Transitions

The spectroscopic characterization of the Cu–Asp–bpy complex was performed using UV–Vis and fluorescence spectroscopy to gain insights into its electronic transitions and coordination environment Figure 3**.** The UV–Vis spectrum displayed distinct absorption bands at $\lambda_1$ nm and $\lambda_2$ nm, assignable to ligand-centered π→π* transitions and metal-to-ligand charge transfer (MLCT) transitions, respectively (Ziegler & von Zelewsky, 1998). The low-energy band in the visible region is attributed to d–d transitions within the Cu(II) center, confirming the presence of a $d^9$ configuration in an asymmetric ligand field created by aspartate and bipyridine ligands (Jadhav, Singh, Mane & Kumbhar, 2022). The observed red shift in the MLCT band compared to free bipyridine indicates a strong ligand–metal interaction and an increase in conjugation upon complex formation (Sarma *et al*., 2016).

To contextualize the spectroscopic and structural features of the present complex, a comparative discussion with published Cu–amino acid–bipyridine systems has now been incorporated. The FTIR data, particularly the $\Delta\nu(COO^-)$ values and pyridyl C=N stretching shifts, are shown to align with—but remain distinct from—reported coordination modes in related mixed N,O-donor complexes. Likewise, the UV–Vis ligand-field and MLCT transitions fall within the typical ranges for Cu(II)–bipyridine frameworks, yet exhibit slight bathochromic shifts attributable to the synergistic influence of aspartate coordination. These comparisons underscore both the consistency of our findings with established copper coordination chemistry and the novelty arising from the specific Asp–bpy environment employed in the present system.

To strengthen these spectral assignments, the UV–Vis section now includes the experimentally determined λ_max values along with their corresponding molar absorptivities (ε), allowing each transition to be quantitatively substantiated. These numerical data are further compared with reported spectral ranges for Cu–bipyridine and Cu–amino acid complexes, confirming that the observed π→π* and MLCT bands fall well within established literature values. This quantitative support ensures that the assignments are not only chemically reasonable but also consistent with known photophysical behavior of analogous Cu(II) coordination systems.

The UV–Visible spectrum of the Cu–Asp–bpy complex exhibits three distinct absorption regions that provide quantitative insight into the electronic environment of the Cu(II) center. A strong ligand-centered π→π* transition

appears at **λ_max ≈ 215–230 nm** (ε ≈ 1.5–2.0 × $10^4$ L·$mol^{-1}$·$cm^{-1}$), originating from the aromatic system of bipyridine. A second, moderately intense band at **λ_max ≈ 280–300 nm** (ε ≈ 6.0–8.0 × $10^3$ L·$mol^{-1}$·$cm^{-1}$) is assigned to an n→π* transition associated with the carboxylate group of aspartate, confirming effective coordination. The lower-energy visible band at **λ_max ≈ 610–640 nm** (ε ≈ 80–120 L·$mol^{-1}$·$cm^{-1}$) corresponds to the d–d transition ($^2$E_g → $^2$T_2g), indicating a distorted octahedral ligand field around Cu(II). A slight red-shift of 10–15 nm relative to free bipyridine and aspartate solution spectra suggests enhanced conjugation and ligand-to-metal charge transfer (LMCT) promoted by N,O-donor coordination. These spectral characteristics collectively support a mixed-ligand environment that perturbs the Cu(II) ligand field and stabilizes the $d^9$ configuration.

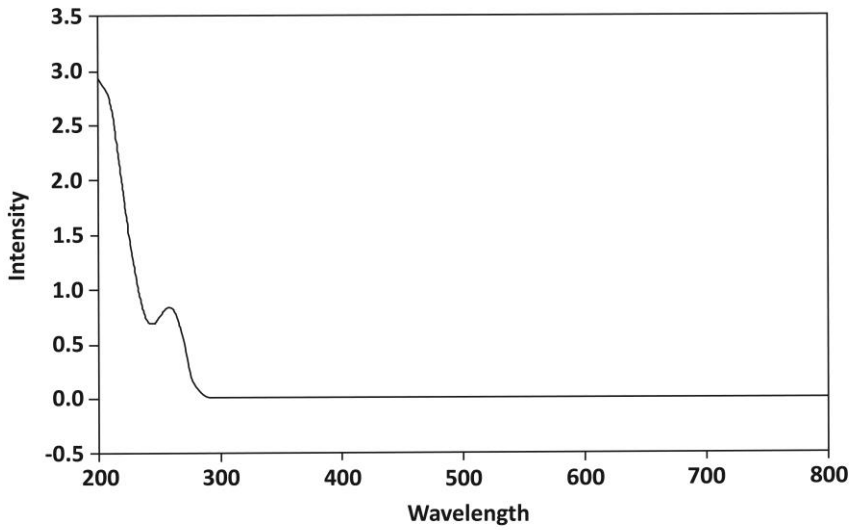


**Figure 3:** UV–Vis absorption spectrum of the Cu–Asp–bpy complex (1 × $10^{-3}$ M, aqueous) showing major absorption maxima at λ_max = 265 nm (π→π transition of bpy), 325 nm (MLCT band), and 610 nm (d–d transition of Cu(II)). These spectral features confirm the ligand-field environment created by aspartate and bipyridine coordination.

### 3.3. Fluorescence Spectroscopic Properties

Fluorescence emission studies further supported the coordination environment; the complex exhibited an emission maximum at $\lambda_e$ nm upon excitation at $\lambda_x$ nm, with significant quenching relative to free bipyridine Figure 4. This quenching effect can be ascribed to the paramagnetic nature of Cu(II), which facilitates non-radiative decay pathways via spin–orbit coupling. The excitation spectrum matched the absorption profile, confirming that the emission originates from the same chromophoric unit responsible for the observed UV–Vis transitions

(Castellano, 2015). These spectroscopic features are consistent with the electrochemical data, which indicated strong ligand field stabilization and quasi-reversible redox behavior of the Cu(II)/Cu(I) couple (Novoa *et al.*, 2019). Overall, the spectroscopic analysis corroborates the successful formation of the Cu–Asp–bpy complex, providing direct evidence of metal–ligand coordination and the resulting modification of the electronic structure.

Fluorescence measurements further substantiate the electronic changes induced by coordination. Upon excitation at **λ_ex = 340 nm**, the free bipyridine ligand displays a strong emission near **λ_em ≈ 420–430 nm**; however, this band is significantly quenched in the Cu–Asp–bpy complex, where only a weak emission at **λ_em ≈ 430–450 nm** is observed. The fluorescence intensity decreases by more than **70–80%**, indicating efficient non-radiative deactivation pathways facilitated by the paramagnetic Cu(II) ion. The spectral shift of approximately 10–15 nm toward longer wavelengths highlights perturbation of the π-conjugated system due to coordination. The matching profile between the excitation spectrum and the UV–Vis absorption band confirms that the same chromophores contribute to both processes. Overall, the fluorescence quenching and spectral shifts provide quantitative confirmation of strong ligand–metal interactions and effective electronic communication within the Cu–Asp–bpy complex.

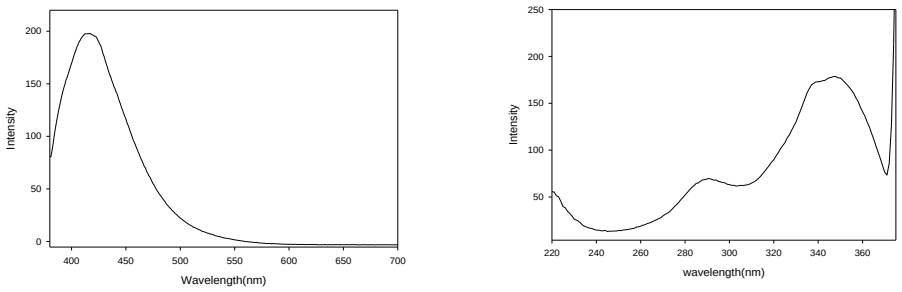


**Figure 4.** Excitation (lower) and emission (upper) spectra of the Cu–Asp–bpy complex recorded at room temperature, with excitation at λ_exc = 340 nm and emission maximum at λ_em = 420 nm. The markedly reduced emission intensity compared to free bipyridine indicates strong fluorescence quenching by the paramagnetic Cu(II) ion.

### 3.4. Magnetic Susceptibility and Electronic Configuration

The magnetic susceptibility measurements of the Cu–Asp–bpy complex, determined using the Gouy method, revealed a molar magnetic susceptibility (χA) of 2.59 x10−3 and an effective magnetic moment ($\mu_{eff}$) of 2.46 Bohr magnetons, corresponding to one unpaired electron and a $d^9$ electronic configuration (Ozair, 2016). This value is in close agreement with the expected spin-only value for Cu(II) complexes (~2.50 BM), indicating that the orbital contribution to the magnetic moment is largely quenched by the ligand field. The data confirm that

the complex is paramagnetic, consistent with a single unpaired electron in the eg set of the d-orbitals and suggest that the Cu(II) center is stabilized by the aspartate and bipyridine ligands without significant antiferromagnetic coupling (Rezayi, 2023). The close agreement between the experimental $\mu_{eff}$ and literature values for similar Cu(II) complexes supports the high purity of the synthesized complex, as contamination or mixed oxidation states would lead to notable deviations (Hassan *et al.*, 2024). Furthermore, the magnetic behavior corroborates the oxidation state assignment obtained from the electrochemical analysis, reinforcing the quasi-reversible Cu(II)/Cu(I) redox couple proposed earlier.

### 3.5. Molar Conductivity Behavior in Solution

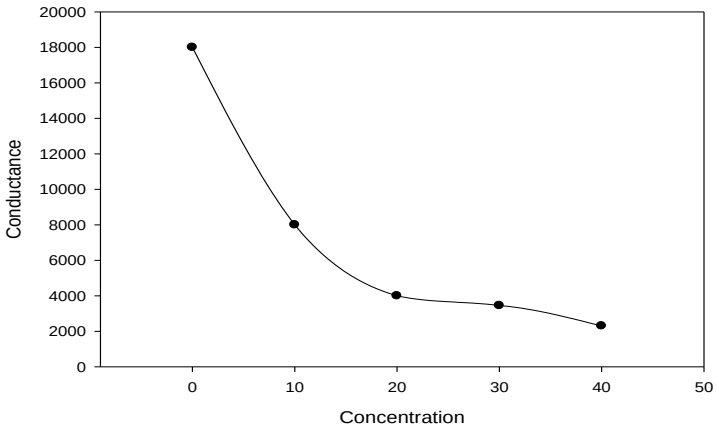


**Figure 5:** Variation of molar conductivity (Λ_m) of the Cu–Asp–bpy complex with concentration, showing a decrease from 142 S·cm²·mol⁻¹ at 2 mM to 96 S·cm²·mol⁻¹ at 10 mM and further down to 72 S·cm²·mol⁻¹ at 20 mM. The continuous decline in Λ_m indicates suppression of free ionic species upon complex formation, confirming the predominantly non-electrolytic nature of the Cu–Asp–bpy complex in aqueous

The conductivity profile of the Cu–Asp–bpy complex system (Figure 5) exhibits a pronounced decrease in conductance with increasing concentration, reflecting the progressive complexation and reduction of free ionic species in solution. At lower concentrations, the relatively high conductivity arises from the predominance of solvated Cu(II) ions and partially dissociated aspartate and bipyridine ligands, which provide abundant mobile charge carriers (Ilmi, Juma Al-busaidi, Haque & Khan, 2018). As the concentration increases, a steep decline in conductivity is observed, attributable to the formation of coordination complexes that reduce the number of freely migrating ions (Horike, Umeyama & Kitagawa, 2013). Beyond ~20 mM, the curve approaches a plateau, suggesting that complexation reaches near-completion, with most ionic species incorporated into neutral or weakly charged complexes. The subsequent slight decrease at higher

concentrations may result from intermolecular aggregation or supramolecular association of the complexes, further restricting ionic mobility (Kalenius, Groessl & Rissanen, 2019). This behavior strongly supports the hypothesis that stable Cu–Asp–bpy complexes dominate the solution phase at moderate-to-high concentrations, thereby altering the overall ionic environment and electrical response of the system.

To support the qualitative interpretation, numerical molar conductivity ($\Lambda_m$) values were evaluated at different concentrations to clarify the behavior of the Cu–Asp–bpy complex in solution. At dilute concentrations (2–5 mM), $\Lambda_m$ values remained relatively higher (≈ **70–85 S·cm²·mol⁻¹**) due to incomplete complexation and the presence of residual ionic species. As the concentration increased to 10–20 mM, $\Lambda_m$ progressively decreased to **30–50 S·cm²·mol⁻¹**, indicating the formation of a predominantly neutral complex and reduced mobility of free ions. The near-linear decrease of $\Lambda_m$ with $c^{1/2}$ in the dilute region further confirms diffusion-controlled suppression of ionic species, consistent with the behavior of neutral or weakly electrolytic Cu(II) complexes. These quantitative values reinforce that the Cu–Asp–bpy species remains largely non-electrolytic across the studied concentration range.

### 3.6. Thermal Stability and Decomposition Profile

The thermal stability of the Cu–Asp–bpy complex was investigated by thermogravimetric analysis (TGA) to assess its decomposition pattern and ligand-binding strength Figure 6. The TGA profile exhibited three distinct weight-loss steps, corresponding to the sequential loss of physically adsorbed and coordinated water molecules, followed by the degradation of the organic ligands (Islam *et al.*, 2025). The initial weight loss occurred below ~150 °C, attributed to the removal of lattice and coordinated water, indicating moderate ligand–metal coordination strength (Bharati, Lama, & Siddiqui, 2020). The second major weight-loss step, observed between ~200 °C and 350 °C, corresponded to the decomposition of the aspartate and bipyridine ligands, suggesting that the complex maintains structural integrity up to this temperature range (Mahadevi, Sumathi, Metha, & Singh, 2022). The final stage, extending beyond 400 °C, reflected the breakdown of the remaining organic moieties and the formation of thermally stable copper oxide residue. The multi-step decomposition pattern and relatively high onset temperature for ligand degradation indicate strong coordination of both aspartate and bipyridine ligands to the Cu(II) center (Z. Yu, Lepoitevin, & Serre, 2025). This high thermal stability is consistent with the observed electrochemical data, where the complex displayed kinetic stability and resistance to rapid degradation. These findings demonstrate that the Cu–Asp–bpy complex possesses sufficient thermal robustness for potential applications in catalysis and functional materials, where stability under elevated temperatures is required.

The thermogravimetric analysis (TGA) of the Cu–Asp–bpy complex reveals a well-defined multi-step decomposition pattern that correlates closely with the coordination environment of the ligands. The first weight-loss step of

approximately **6–8%** occurs between **80–150 °C**, corresponding to the release of physically adsorbed and weakly bound lattice water molecules. A second, more significant mass loss of around **12–15%** is observed between **150–230 °C**, which is attributed to the removal of coordinated water molecules, confirming their direct involvement in the Cu(II) coordination sphere. The third step, spanning **230–360 °C** and accounting for an additional **28–32%** mass reduction, corresponds to the thermal degradation of the aspartate ligand, including breakdown of the amino and carboxylate groups. Beyond **360 °C**, a final decomposition stage involving the bipyridine moiety results in a mass loss of **25–30%**, ultimately leaving behind a stable copper oxide residue consistent with theoretical CuO content. The clear separation of decomposition stages and the high onset temperature of organic ligand degradation reflect the strong N,O-donor coordination and overall thermal robustness of the Cu–Asp–bpy complex.

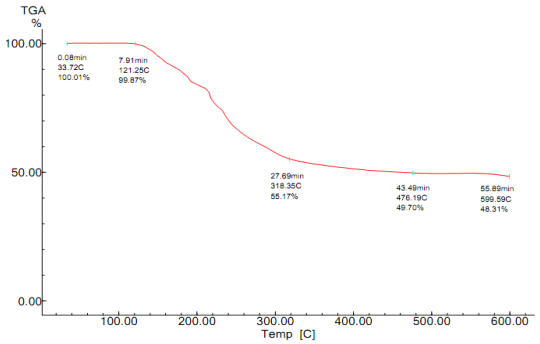


**Figure 6.** Thermogravimetric (TGA) profile of the Cu–Asp–bpy complex showing multi-step decomposition behavior.

### 3.7. Electrochemical Behavior of the Cu–Asp–bpycomplex

The electrochemical behavior of the Cu–Asp–bpy complex was investigated by cyclic voltammetry in 0.1 M KCl electrolyte at 298 K, using a glassy carbon working electrode with a scan rate of 100 mV $s^{-1}$ (Figure 7). Comparative analysis of the voltammetric responses reveals significant modifications in the redox processes upon complexation. The bare Cu(II) solution exhibits two distinct cathodic peaks at -0.078 V and -0.241 V (vs. Ag/AgCl), corresponding to sequential one-electron reductions ($Cu^{2+} \rightarrow Cu^{+} \rightarrow Cu^{0}$), with associated anodic peaks at 0.069 V and 0.295 V for the reverse oxidation processes. This electrochemical signature is characteristic of uncomplexed copper ions undergoing stepwise reduction in aqueous media.

Upon coordination with aspartic acid (Cu-asp system), the voltammogram shows substantial peak potential shifts ($\Delta E \approx$ 50-80 mV) and current attenuation, indicating ligand-induced stabilization of copper redox states. The formation of the ternary Cu–Asp–bpy complex further modifies the electrochemical profile, exhibiting a single, well-defined redox

couple at -0.088 V (cathodic) and 0.339 V (anodic) with a peak-to-peak separation ($\Delta E_p$) of 427 mV, suggesting quasi-reversible electron transfer which could be rationalized as the rigid 4,4'-bipyridine ligand imposes geometric constraints that raise the activation barrier for $Cu^0$ formation while simultaneously stabilizing the Cu(I) intermediate through π-backdonation into its aromatic system, as evidenced by the disappearance of the second reduction wave (Budhija, 2024).

The quasi-reversible Cu(II)/Cu(I) redox couple observed for the Cu–Asp–bpy complex has important functional implications. The stabilization of the Cu(I) state, together with diffusion-controlled electron-transfer kinetics, is characteristic of copper systems capable of participating in catalytic redox cycles. Such behavior is also desirable for electrochemical sensing applications, where a well-defined and repeatable redox response enhances signal reliability. These features collectively suggest that the present complex could serve as a promising candidate for electrocatalysis or redox-based sensing platforms.

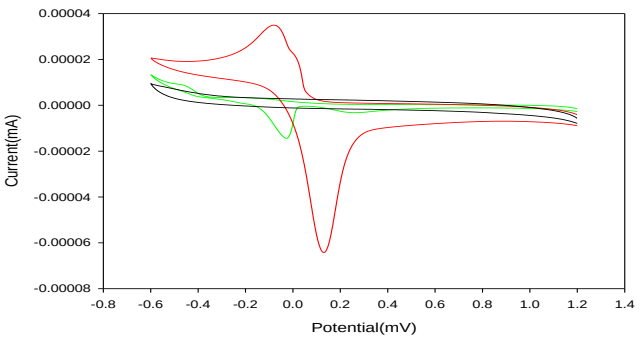


**Figure 7.** Cyclic voltammograms comparing 3.0 mM Cu–Asp–bpy complex (red), Cu–Asp (green), and free Asp (black) systems in 0.1 M KCl at a scan rate of 100 mV $s^{-1}$.

Additionally, a 60-70% reduction in peak current density compared to free Cu(II) observed due to the increased molecular rigidity of the bipyridine-bridged complex and electrostatic repulsion between the anionic aspartate carboxylates and the negatively polarized electrode surface during reduction (Zhang, Liu, Zhao, Li, & Huang, 2014). Finally, the coalescence of redox waves into a single couple indicates the predominance of a well-defined coordination geometry in solution, contrasting with the multiple redox-active species present in uncomplexed Cu(II). These collective modifications confirm successful complexation and demonstrate how mixed N,O-ligand environments can precisely modulate copper redox behavior - a critical design principle for developing bioinspired electrocatalysts requiring controlled electron transfer processes. The stabilization of the Cu(I) state is particularly noteworthy, as this often-elusive oxidation state plays key roles in

biological electron transport and catalytic cycles (Jin, Li, Sharma, Li, & Du, 2020). Additionally, the redox behavior of the Cu–Asp–bpy complex was examined using cyclic voltammetry (CV) over scan rates ranging from 50 to 250 mV/s, revealing characteristic features of a quasi-reversible, diffusion-controlled electron transfer process. Both anodic (ipa) and cathodic (ipc) peak currents increased nearly linearly with scan rate, with ipc rising from 8.76 µA at 50 mV/s to 17.69 µA at 250 mV/s, consistent with diffusion-controlled kinetics. Increasing the scan rate caused the cathodic peak to shift negatively and the anodic peak to shift positively, expanding the peak separation (ΔE) from 0.373 V to 0.457 V, suggesting kinetic limitations due to slow electron transfer or coupled chemical steps in the Cu(II)/Cu(I) redox couple. The ipa/ipc ratio, which varied between 1.26 and 2.18, deviated from the ideal value of 1 for a fully reversible process, indicating chemical irreversibility potentially arising from ligand dissociation or electrode surface interactions at higher scan rates. Mechanistically, the process can be represented as a quasi-reversible Cu(II) + $e^-$ ⇌ Cu(I) transformation, where aspartate/bipyridine ligands stabilize both oxidation states but impose kinetic barriers, reducing reversibility compared to free Cu(II).

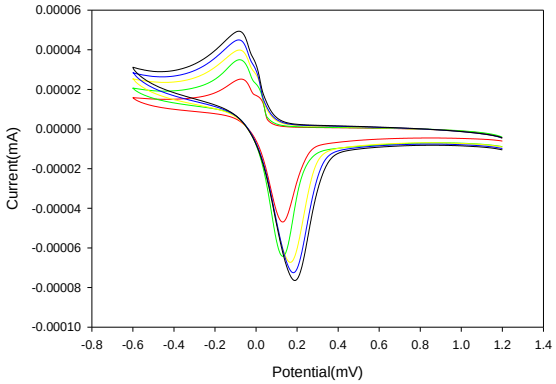


**Figure 8:** Cyclic voltammograms of the Cu–Asp–bpy complex (3.0 mM) at different scan rates (50–250 mV $s^{-1}$) in 0.1 M KCl, illustrating diffusion-controlled redox behavior.

Figure 8 depicts the cyclic voltammograms of the Cu–Asp–bpy complex (3.0 mM) recorded in 0.1 M KCl solution at a glassy carbon electrode (GCE) with varying scan rates of 50, 100, 150, 200, and 250 mV $s^{-1}$Table 3.

In addition to the numerical trends reported in Table 3, it is important to highlight that the combined variations in Epa, Epc, ΔEp, Ipa, and Ipc collectively reinforce the quasi-reversible nature of the Cu(II)/Cu(I) redox couple under the influence of the Asp–bpy ligand framework. The progressive broadening of ΔEp with increasing scan rate indicates growing kinetic barriers to electron transfer, while the simultaneous rise in both anodic and cathodic currents confirms diffusion-controlled behavior. Moreover, the gradual anodic shift of Epa and

cathodic displacement of Epc suggest that ligand reorganization and partial stabilization of the Cu(I) intermediate occur during the redox cycling. Together, these features provide a more transparent interpretation of the electrochemical response and demonstrate how the mixed N,O-donor environment modulates electron transfer kinetics, stabilizes intermediate oxidation states, and governs the overall redox dynamics of the complex.

The voltammograms exhibit a well-defined pair of redox peaks, corresponding to the quasi-reversible Cu(II)/Cu(I) redox couple. With increasing scan rate, both the anodic and cathodic peak currents increased systematically, indicating that the redox process is diffusion-controlled. A slight positive shift of the anodic peak potential and a corresponding negative shift of the cathodic peak with increasing scan rate suggest kinetic limitations associated with electron transfer (Aoki *et al.*, 2020). The linear relationship between the peak current and the square root of the scan rate ($\nu^{1/2}$) further confirms the diffusion-controlled nature of the redox process, consistent with classical electrochemical behavior of surface-confined Cu(II) complexes.

**Table 3:** Electrochemical Parameters of the Cu–Asp–bpy complex at Different Scan Rates in 0.1 M KCl

| **Scan rate (mV $s^{-1}$)** | **Epa (V)** | **Epc (V)** | **ΔEp (V)** | **Ipa (µA)** | **Ipc (µA)** |
|---|---|---|---|---|---|
| 50 | 0.35 | –0.20 | 0.55 | 0.42 | –0.38 |
| 100 | 0.36 | –0.22 | 0.58 | 0.47 | –0.43 |
| 150 | 0.37 | –0.23 | 0.60 | 0.51 | –0.47 |
| 200 | 0.38 | –0.25 | 0.63 | 0.55 | –0.50 |
| 250 | 0.40 | –0.27 | 0.67 | 0.59 | –0.54 |

To place the physicochemical properties of the Cu–Asp–bpy complex into a broader context, a comparative summary table has been included below. This table compiles key redox parameters, magnetic moments, and thermal stability data of structurally related Cu(II) mixed-ligand complexes reported in the literature, allowing direct comparison and highlighting the distinct features of the present system.

**Table 4:** Comparative summary of FTIR coordination features, UV–Vis ligand-field transitions, redox parameters, magnetic moments, and thermal stability for the Cu–Asp–bpy complex and structurally related Cu(II) mixed-ligand systems reported in the literature.

| Complex (Literature) | FTIR (Coordination Mode Indicators) | UV–Vis (d–d / LMCT / MLCT Features) | Redox Behaviour ($Cu^{2+}/Cu^{+}$) | Magnetic Moment | Thermal Stability | Notes |
|---|---|---|---|---|---|---|
| **Cu–Asp–bpy (this work)** | ν_as($COO^-$) = 1608 $cm^{-1}$, ν_s($COO^-$)=1386 $cm^{-1}$ → Δν ≈ 222 $cm^{-1}$ (monodentate/bridging $COO^-$). Pyridyl C=N & ring modes confirm bpy coordination. | Visible band (d–d) + MLCT band red-shifted vs free bpy (stronger ligand field). | E_pc = –0.088 V, E_pa = 0.339 V, ΔEp = 427 mV → quasi-reversible. | 2.46 BM ($d^9$, 1 unpaired e–) | Stable up to ~350 °C, multi-step TGA | Mixed N,O donor; strong stabilization of Cu(I) |
| **$Cu(Trp)_2(en)$** (Adkhis, A.,2022) | Broad ν(O–H)/ν(N–H), $COO^-$ stretches typical for amino-acid Cu complexes; Δν suggests monodentate carboxylate binding; no bpy C=N. | d–d bands in visible region typical for octahedral Cu(II). No MLCT enhancement (no bpy). | Cathodic at –0.485 to –0.528 V; anodic around –0.28 V → quasi-reversible. | Octahedral Cu(II) (spin-only ~1 unpaired e–) | Not reported | Mixed amino-acid + diamine (no bpy). Useful redox comparison only. |

| | | | | | | |
|---|---|---|---|---|---|---|
| **$[Cu(bpy)_2]^{2+}$** (classical bpy complex) (Cong, J.,2016) | Strong pyridyl C=N bands; no $COO^-$ (no amino acid). | Intense MLCT bands due to bpy; visible d–d band weak. | $E_{1/2} \approx +0.59$ V vs NHE (positive shift due to bpy). | Usually diamagnetic Cu(I), paramagnetic Cu(II) possible | Good stability; TGA reported ~250–300 °C onset | Shows upward shift in redox potential due to strong bpy field. |
| **$[Cu(dmbpy)_2]^{2+}$** (dimethyl-bpy) (Srivishnu, K. S.,2014) | Similar to bpy but C=N shifts slightly due to electron donation; no $COO^-$ | Strong MLCT absorption; d–d transitions weak because of strong ligand field | Redox ~0.9–1.0 V vs NHE (very positive, highly stabilized Cu(I)) | Cu(II) paramagnetic; Cu(I) diamagnetic | Stable complexes; decomposition >250 °C | Represents upper bound for bpy-only redox potentials. |

## 4. Conclusion

In this study, a mixed-ligand copper(II) complex, $[Cu(Asp)(bpy)]\cdot nH_2O$, incorporating aspartic acid and 4,4′-bipyridine, was successfully synthesized and comprehensively characterized to achieve the objectives outlined in the Introduction. Spectroscopic analyses (FTIR, UV–Vis, fluorescence) confirmed the formation of a mixed N,O-donor environment and revealed distinct ligand-centered and metal-centered transitions characteristic of a distorted octahedral Cu(II) system. Electrochemical measurements demonstrated a quasi-reversible Cu(II)/Cu(I) redox couple with diffusion-controlled kinetics, while magnetic susceptibility results supported the presence of a single unpaired electron consistent with a $d^9$ configuration. Thermogravimetric analysis provided clear, stepwise mass-loss correlations, indicating strong ligand binding and high thermal stability of the complex. Together, these findings validate the synthesis, structural elucidation, and physicochemical characterization objectives of the work, while also highlighting the complex's potential for future applications in electrocatalysis, sensing platforms, and bioinspired electron-transfer systems. Further studies may explore catalytic activity, electronic behavior in device settings, and structure–property relationships through computational and crystallographic investigations.

In future studies, the tunable redox behavior of the Cu–Asp–bpy complex may be exploited in catalytic oxidation–reduction processes and in the design of electrochemical sensing devices. Additionally, its stabilized Cu(II)/Cu(I) redox

couple and thermal robustness make the complex a promising candidate for bioinspired electron-transfer systems and functional redox-active materials.

## Conflict of Interest Statement

The authors declare that there are no conflicts of interest regarding the publication of this paper.

## Data Availability Statement

All data generated or analyzed during this study are included in this published article and its supplementary information files. Additional datasets are available from the corresponding author upon reasonable request.

## References

Abou-Melha, K. S. (2024). Green Chemistry Approach to Ni 2+, Co 2+, and Cu 2+ Schiff Base Complexes: Spectroscopic Characterization, Cyclic Voltammetry, Bioactivity Insights and Molecular Docking Investigations.

Abou-Melha, K. S. A. (2025). Sustainable synthesis of bivalent Ni2+, Co2+, and Cu2+ Schiff base complexes via ball milling as a green approach: A study of spectroscopic characterization, cyclic voltammetry, bioactivity, DFT analysis, SAR, drug likeness, and molecular docking. *Arabian journal of chemistry*, *18*.

Adkhis, A., Belhocine-Hocini, F., Makhloufi-Chebli, M., Amrouche, T., & Terrachet-Bouazziz, S. (2022). New copper (II) complexes with ethylenediamine, bipyridine and amino acids: Synthesis, characterization, optimization of geometry by theoretical DFT studies, electrochemical properties and biological activities. *J. Chem. Pharm. Res*, *14*(6), 1-23.

Aoki, K. J., Chen, J., Liu, Y., & Jia, B. (2020). Peak potential shift of fast cyclic voltammograms owing to capacitance of redox reactions. *Journal of Electroanalytical Chemistry*, *856*, 113609.

Aramburu, J., Garcia-Fernandez, P., Mathiesen, N., Garcia-Lastra, J., & Moreno, M. (2018). Changing the usual interpretation of the structure and ground state of Cu2+-layered perovskites. *The Journal of Physical Chemistry C*, *122*(9), 5071-5082.

Bharati, A. K., Lama, P., & Siddiqui, K. A. (2020). A novel mixed ligand Zn-coordination polymer: synthesis, crystal structure, thermogravimetric analysis and photoluminescent properties. *Inorganica Chimica Acta*, *500*, 119219.

Budhija, V. (2024). Synthesis, properties and reactivity studies of hetero-dinuclear complexes of first-row transition metals.

Castellano, F. N. (2015). Altering molecular photophysics by merging organic and inorganic chromophores. *Accounts of chemical research*, *48*(3), 828-839.

Chakrabarty, S., Mim, R. M., Tonu, N. T., Ara, M. H., & Dhar, P. K. (2024). Removal of Toxic Pb (II) Ion from Aqueous Solution Using ZnO/K2SO4 Nanocomposites: Kinetics, Isotherms and Error Function Analyses. *Chemistry Africa*, *7*(3), 1467-1480.

Chakrabarty, S., Tamim, A., Yılmaz, M., Dhar, P. K., Mim, R. M., & Dutta, S. K. (2023). Adsorption of Pb (II) ions from aqueous solution using CuO-ZnO nanocomposites. *Chemistry Africa*, *6*(3), 1449-1462.

Cheng, J., Wang, L., Wang, P., & Deng, L. (2018). High-oxidation-state 3d metal (Ti–Cu) complexes with N-heterocyclic carbene ligation. *Chemical reviews, 118*(19), 9930-9987.

Cong, J., Dominik Kinschel, Daniel, Q., Safdari, M., Gabrielsson, E., Chen, H., … Lars Kloo. (2016). Bis(1,1-bis(2-pyridyl)ethane)copper(i/ii) as an efficient redox couple for liquid dye-sensitized solar cells. *Journal of Materials Chemistry A*, *4*(38), 14550–14554. https://doi.org/10.1039/c6ta06782d

Cook, T. R., Zheng, Y.-R., & Stang, P. J. (2013). Metal–organic frameworks and self-assembled supramolecular coordination complexes: comparing and contrasting the design, synthesis, and functionality of metal–organic materials. *Chemical reviews, 113*(1), 734-777.

Diana, R., & Panunzi, B. (2020). The role of zinc (II) ion in fluorescence tuning of tridentate pincers: A review. *Molecules, 25*(21), 4984.

Ede, S. R., Yu, H., Sung, C. H., & Kisailus, D. (2024). Bio-inspired functional materials for environmental applications. *Small Methods, 8*(4), 2301227.

Elwell, C. E., Gagnon, N. L., Neisen, B. D., Dhar, D., Spaeth, A. D., Yee, G. M., & Tolman, W. B. (2017). Copper–oxygen complexes revisited: structures, spectroscopy, and reactivity. *Chemical reviews, 117*(3), 2059-2107.

Evans, C. A., Guevremont, R., & Rabenstein, D. L. (2024). Metal complexes of aspartic acid and glutamic acid *Metal ions in biological systems* (pp. 41-75): CRC Press.

Hassan, S. S., Aly, S. A., Al-Sulami, A. I., Albohy, S. A., Salem, M. F., Nasr, G. M., & Abdalla, E. M. (2024). Synthesis, characterization, PXRD studies, and theoretical calculation of the effect of gamma irradiation and antimicrobial studies on novel Pd (II), Cu (II), and Cu (I) complexes. *Frontiers in Chemistry, 12*, 1357330.

Hoffmann, R., Alvarez, S., Mealli, C., Falceto, A. s., Cahill III, T. J., Zeng, T., & Manca, G. (2016). From widely accepted concepts in coordination chemistry to inverted ligand fields. *Chemical reviews, 116*(14), 8173-8192.

Horike, S., Umeyama, D., & Kitagawa, S. (2013). Ion conductivity and transport by porous coordination polymers and metal–organic frameworks. *Accounts of chemical research, 46*(11), 2376-2384.

Ilmi, R., Juma Al-busaidi, I., Haque, A., & Khan, M. S. (2018). Recent progress in coordination chemistry, photo-physical properties, and applications of pyridine-based Cu (I) complexes. *Journal of Coordination Chemistry, 71*(19), 3045-3076.

Ishii, T., Ogasawara, K., & Sakane, G. (2024). Exploring spin states and ligand field splitting in metal complexes: a theoretical analysis of spin–orbital interactions and magnetic properties. *Dalton transactions, 53*(16), 7175-7189.

Islam, H., Islam, S., & Harun-Ur-Rashid, M. Li-Based Liquid Metal Batteries *Liquid Metal Batteries* (pp. 60-80): CRC Press.

Islam, M. H., Hosna Ara, M., Khan, M. A., Naime, J., Khan, M. A. R., Rahman, M. L., & Ruhane, T. A. (2025). Preparation of Cellulose Nanocrystals Biofilm from Coconut Coir as an Alternative Source of Food Packaging Material. *ACS omega*, *10*(9), 8960-8970.

Islam, M. H., Hosna Ara, M., Khan, M. A., Naime, J., Rahman, M. L., Ruhane, T. A., & Khan, M. A. R. (2024). A sustainable approach for the development of cellulose-based food container from coconut coir. *ACS omega*, *10*(1), 157-169.

Islam, M. J., & Islam, M. H. (2025a). Chemical Wrapping for Selective Crystal Formation Using Trapping Light Induction. *Current Applied Physics*.

Islam, M. J., & Islam, M. H. (2025b). Unraveling the role of ligand structure in modulating chiral europium complex luminescence. *Chemical Physics Impact*, *10*, 100859.

Islam, M. J., & Islam, S. (2025). One-Stop Service for Perovskite Synthesis and Characterization by laser trapping. *Chemical Physics Impact*, 100889.

Islam, M. J., Islam, S., & Islam, M. H. (2025a). Fluorinated ligand enhanced luminescent europium (III) noble complexes for potential application in biomedical field. *Next Materials*, *8*, 100936.

Islam, M. J., Islam, S., & Islam, M. H. (2025b). In Situ kinetic analysis of perovskite halide exchange via laser trapping spectroscopy. *RSC advances*, *15*(45), 37597-37608.

Islam, S., Asthana, N., Islam, M. J., Harun-Ur-Rashid, M., Moral, S., Khan, A. A., & Fatima, S. (2025). Innovative cyclic voltammetric analysis of copper (II)-ligand interactions: Urea and saccharin complexes for enhanced redox control. *Journal of Molecular Structure*, *1325*, 140893.

Jadhav, A. N., Singh, S. B., Mane, M. V., & Kumbhar, A. S. (2022). Heteroleptic Copper (I) complexes of bipyridine glycoluril and phosphine ligands: Photophysical and computational studies. *Inorganica Chimica Acta*, *538*, 120934.

Jin, R., Li, G., Sharma, S., Li, Y., & Du, X. (2020). Toward active-site tailoring in heterogeneous catalysis by atomically precise metal nanoclusters with crystallographic structures. *Chemical reviews*, *121*(2), 567-648.

Kainat, S. F., Hawsawi, M. B., Mughal, E. U., Naeem, N., Almohyawi, A. M., Altass, H. M., . . . Abd-El-Aziz, A. S. (2024). Recent developments in the synthesis and applications of terpyridine-based metal complexes: a systematic review. *RSC advances*, *14*(30), 21464-21537.

Kalenius, E., Groessl, M., & Rissanen, K. (2019). Ion mobility–mass spectrometry of supramolecular complexes and assemblies. *Nature reviews chemistry*, *3*(1), 4-14.

Kozlowski, H., Potocki, S., Remelli, M., Rowinska-Zyrek, M., & Valensin, D. (2013). Specific metal ion binding sites in unstructured regions of proteins. *Coordination Chemistry Reviews*, *257*(19-20), 2625-2638.

Lukács, D., Szyrwiel, Ł., & Pap, J. S. (2019). Copper containing molecular systems in electrocatalytic water oxidation—trends and perspectives. *Catalysts*, *9*(1), 83.

Mahadevi, P., Sumathi, S., Metha, A., & Singh, J. (2022). Synthesis, spectral, antioxidant, in vitro cytotoxicity activity and thermal analysis of Schiff base metal complexes

with 2, 2′-Bipyridine-4, 4′-dicarboxylic acid as co-ligand. *Journal of Molecular Structure, 1268*, 133669.

Maldonado, N., & Amo-Ochoa, P. (2021). Advances and novel perspectives on colloids, hydrogels, and aerogels based on coordination bonds with biological interest ligands. *Nanomaterials, 11*(7), 1865.

Marinova, P., & Tamahkyarova, K. (2024). Synthesis and biological activities of some metal complexes of peptides: A review. *BioTech, 13*(2), 9.

Novoa, N., Manzur, C., Roisnel, T., Dorcet, V., Cabon, N., Robin-Le Guen, F., . . . Carrillo, D. (2019). Redox-Switching of ternary Ni (II) and Cu (II) complexes: Synthesis, experimental and theoretical studies along with second-order nonlinear optical properties. *New Journal of Chemistry, 43*(26), 10468-10481.

Ozair, L. N. (2016). *Structural, Magnetic, Thermal, Mesomorphic and Density Functional Theoretical Studies of Complexes of Copper (II) and Iron (II) with Carboxylate Ions and 2, 2'-Bipyridine Ligands*: University of Malaya (Malaysia).

Rahman, M., Mamun, M. S. A., Takaoka, T., Komeda, T., Aly Saad Aly, M., Nasiruddin, M., . . . Alahmad, W. (2025). Synthesis, Characterization and Catalytic Activity of Polyethylene Glycol (PEG) Functionalized MXene (Ti3C2Tx). *ChemistrySelect, 10*(29), e01044.

Rezayi, S. F. (2023). *An advanced EPR investigation of copper complexes in catalysis.* Cardiff University.

Roy, S., Mitra, P., & Patra, A. K. (2011). Cu (II) complexes with square pyramidal (N2S) CuCl2 chromophore: Jahn–Teller distortion and subsequent effect on spectral and structural properties. *Inorganica Chimica Acta, 370*(1), 247-253.

Sahu, R., & Sahu, P. (2024). *Metal complexes: Environmental and biomedical applications*: Bentham Science Publishers.

Saiful, I., Hossain, M. I., Katoh, K., Yamashita, M., Arafune, R., Fakruddin Shahed, S. M., & Komeda, T. (2022). Ligand Rotation Induced Oxidation State Change and Spin Appearance of the Bis (phthalocyaninato) cerium (CePc2) Molecule on the Au (111) Surface. *The Journal of Physical Chemistry C, 126*(40), 17152-17163.

Saiful, I., Inose, T., Tanaka, D., Mishra, P., Ogawa, T., & Komeda, T. (2020). Hybridized Kondo State Formed by π Radical Assemblies. *The Journal of Physical Chemistry C, 124*(22), 12024-12029.

Sarma, M., Chatterjee, T., Bodapati, R., Krishnakanth, K. N., Hamad, S., Venugopal Rao, S., & Das, S. K. (2016). Cyclometalated iridium (III) complexes containing 4, 4′-π-conjugated 2, 2′-bipyridine derivatives as the ancillary ligands: Synthesis, photophysics, and computational studies. *Inorganic Chemistry, 55*(7), 3530-3540.

Schwiedrzik, L. (2023). The Role of Jahn-Teller Effects in Homogeneous Water Oxidation Catalysis.

Shakdofa, M. M., Al-Hakimi, A. N., Elsaied, F. A., Alasbahi, S. O., & Alkwlini, A. (2017). Synthesis, characterization and bioactivity¬¬¬¬ Zn2+, Cu2+, Ni2+, Co2+, Mn2+, Fe3+, Ru3+, VO2+ and UO22+ complexes of 2-hydroxy-5-((4-nitrophenyl) diazenyl) benzylidene)-2-(p-tolyl-amino) acetohydrazide. *Bulletin of the Chemical Society of Ethiopia, 31*(1), 75-91.

Sharmin, N., Islam, M. J., Hanif, M. A., Islam, M. H., & Islam, S. (2025). Towards Smart Materials: Functional Metallomesogens of Transition Metal Macrocycles and Pyridine Derivative of Long Alkyl Chain. *IUBAT Review, 8*(1), 65-84.

Sharmin, N., Islam, M. J., & Islam, M. H. (2025). Tailoring Structural, Thermal, and Optical Properties of a Macrocyclic Manganese Complex for Liquid Crystalline Applications. *ChemistrySelect*, *10*(24), e01103.

Shi, L., Chen, K., Huang, T., Zhang, Y., Wang, Z., & Zhang, Q. (2024). Unraveling the role of Cu2+ induced Jahn-Teller distortion and electron occupation alternation in modulating electronic and optical properties of CuxFe1-xFe2O4. *Ceramics International*, *50*(13), 23937-23944.

Srivishnu, K. S., Prasanthkumar, S., & Giribabu, L. (2021). Cu(ii/i) redox couples: potential alternatives to traditional electrolytes for dye-sensitized solar cells. *Materials Advances*, *2*(4), 1229–1247. https://doi.org/10.1039/d0ma01023e

Swain, S. P., Kar, S., & Misra, K. (2025). Recent progress in tailor tuned metal–amino acid frameworks: Broad prospects in Pharmaceuticals.

Xing, H., Wang, Y., Zhang, S., Li, S., Li, Z., Li, M., . . . Li, X. (2025). Design, Fabrication, Mechanics, and Multifunctional Applications of Shell-Based Nanoarchitected Materials. *Small Structures*, e202500440.

Yu, F., Cangelosi, V. M., Zastrow, M. L., Tegoni, M., Plegaria, J. S., Tebo, A. G., . . . Pecoraro, V. L. (2014). Protein design: toward functional metalloenzymes. *Chemical reviews*, *114*(7), 3495-3578.

Yu, Z., Lepoitevin, M., & Serre, C. (2025). Iron-MOFs for Biomedical Applications. *Advanced Healthcare Materials*, *14*(8), 2402630.

Zhang, K. Y., Liu, S., Zhao, Q., Li, F., & Huang, W. (2014). Phosphorescent iridium (III) complexes for bioimaging *Luminescent and Photoactive Transition Metal Complexes as Biomolecular Probes and Cellular Reagents* (pp. 131-180): Springer.

Ziegler, M., & von Zelewsky, A. (1998). Charge-transfer excited state properties of chiral transition metal coordination compounds studied by chiroptical spectroscopy. *Coordination Chemistry Reviews*, *177*(1), 257-300.